Postprint of: Soil Biology and Biochemistry 77: 1-11 (2014)

Working title: Factors affecting the molecular structure and mean residence time of occluded organics in a lithosequence of soils under ponderosa pine

Katherine Heckman[a*], Heather Throckmorton[b], Christopher Clingensmith[a], Francisco Javier González Vila[c], William R Horwath[b], Heike Knicker[c], and Craig Rasmussen[a],

*Corresponding Author Current affiliation & address:
USDA Forest Service, Northern Research Station
Center for Accelerator Mass Spectrometry, LLNL
Address:
CAMS, L-397
Lawrence Livermore National Lab
7000 East Ave
Livermore, CA 94550, USA
kaheckman@fs.fed.us
phone : +1 925 422 9556
fax : +1 925 423 7884

[a] Dept. of Soil, Water & Environmental Science
University of Arizona
PO Box 210038
Tucson, AZ 85721-0038, USA
phone: +1 520 621 1646
fax: +1 520 621 1647
crasmuss@cals.arizona.edu
c.clingensmith.ufl@gmail.com

[b] Dept. Land, Air and Water Resources
University of California, Davis
One Shields Ave
Davis, CA 95616, USA
phone: +1 754-6185
fax: +1 752-1552
wrhorwath@usdavis.edu
hthrockmorton@lanl.gov

[c] Instituto de Recursos Naturales y Agrobiología de Sevilla
Consejo Superior de Investigaciones Científicas
Avenida Reina Mercedes 10
41080 Seville, Spain
phone: +34 95 462 4711
fax: +34 95 462 4002
knicker@irnase.csic.es
fjgon@irnase.csic.es

Keywords: occluded organic matter, forest soil, soil organic matter, density fractionation, black carbon

1

Abstract

Occluded, or intra-aggregate, soil organic matter (SOM) comprises a significant portion of the total C pool in forest soils and often has very long mean residence times (MRTs). However, occluded C characteristics vary widely among soils and the genesis and composition of the occluded organic matter pool are not well understood. This work sought to define the major controls on the composition and MRT of occluded SOM in western U.S. conifer forest soils with specific focus on the influence of soil mineral assemblage and aggregate stability. We sampled soils from a lithosequence of four parent materials (rhyolite, granite, basalt, and dolostone) under *Pinus ponderosa*. Three pedons were excavated to the depth of refusal at each site and sampled by genetic horizon. After density separation at 1.8 g cm^{-3} into free/light, occluded and mineral fractions, the chemical nature and mean residence time of organics in each fraction were compared. SOM chemistry was explored through the use of stable isotope analyses, ^{13}C NMR, and pyrolysis GC/MS. Soil charcoal content estimates were based on ^{13}C NMR analyses. Estimates of SOM MRT were based on steady-state modelling of SOM radiocarbon abundance measurements. Across all soils, the occluded fraction was 0.5-5 times enriched in charcoal in comparison to the bulk soil and had a substantially longer MRT than either the mineral fraction or the free/light fraction. These results suggest that charcoal from periodic burning is the primary source of occluded organics in these soils, and that the structural properties of charcoal promote its aggregation and long-term preservation. Surprisingly, aggregate stability, as measured through ultrasonic dispersion, was not correlated with occluded SOM abundance or MRT, perhaps raising questions of how well laboratory measurements of aggregate stability capture the dynamics of aggregate turnover under field conditions. Examination of the molecular

characteristics of the occluded fraction was more conclusive. Occluded fraction composition did not change substantially with soil mineral assemblage, but was increasingly enriched in charcoal with depth relative to bulk SOM. Enrichment levels of ^{13}C and ^{15}N suggested a similar degree of microbial processing for the free/light and occluded fractions, and molecular structure of occluded and free/light fractions were also similar aside from charcoal enrichment in the occluded fraction. Results highlight the importance of both fire and aggregate formation to the long-term preservation of organics in western U.S. conifer forests which experience periodic burning, and suggest that the composition of occluded SOM in these soils is dependent on fire and the selective occlusion of charcoal.

1. Introduction

Temperate forest soils contain a substantial portion of the global terrestrial C pool, and gaining the ability to accurately model forest soil C dynamics is important for the improvement of both regional and global C cycle models. The soil organic C cycle has been the subject of intense study in recent decades (e.g. Kögel-Knabner and Kleber, 2011), but considerable knowledge gaps remain. One such knowledge gap is the identification of the mechanisms and/or characteristics of occluded organic matter which lead to its persistence in soils. Here we specifically address this knowledge gap through quantifying the physical partitioning, chemistry, and residence time of soil C in a range of temperate conifer forests in the Southwest U.S.

The SOM pool encompasses a high degree of heterogeneity in both molecular structure and mean residence time (MRT). Particulate organics found within the mineral soil matrix, but outside aggregate structures, strongly resemble local plant inputs, and tend to have a comparably short MRT. Organic compounds intimately associated with mineral particles are often compositionally more similar to microbial necromass than plant inputs, and usually have comparably longer MRTs due to chemical protection against biodegradation. Occluded SOM, or aggregate-protected particulate organic matter, is assumed to be physically protected from biodegradation through association with soil minerals, but occluded organics vary widely in both composition and MRT (von Lützow et al., 2006, 2007; Kögel-Knabner and Kleber, 2011).

Isolation of occluded organics from mineral-associated (mineral/heavy fraction) and particulate (free/light) organics is usually achieved through density separation in combination with aggregate disruption (Golchin et al., 1994; Sohi et al., 2001; Swanston et al., 2003). Density separation allows for the separation of organics adhered to mineral surfaces (mineral fraction) from organics unassociated with the mineral

component (free/light fraction). The incorporation of aggregate disruption into density separation methods (achieved through sonication or crushing) allows for the isolation of the occluded fraction of SOM, or SOM protected through occlusion within aggregate structures and/or coating with mineral grains. Though these methods have their limitations (Crow et al., 2007), they have been shown to effectively isolate unique pools of SOM with distinct differences in MRT (e.g., Rasmussen et al, 2005).

The occluded fraction comprises a significant portion of the total organic matter pool in forest soils, with some estimates as high as 40-50% of total soil C (Rasmussen et al., 2005; Wagai et al., 2008). However, the genesis and composition of occluded organics are not well understood. In a summary of contemporary investigations, Wagai et al. (2009) noted several trends in occluded SOM characteristics. Occluded organics typically have a smaller particle size than organics in the free/light fraction, ranging from 10-100 μm. Occluded organics generally lack recognizable features of plant fragments, and the occluded fraction tends to accumulate structurally recalcitrant compounds such as pollen, fungal spores and charred materials. Wagai et al. (2009) reported C:N ratios of occluded organics ranging from 13 to 88, and MRTs of ~50 to >1,000 years.

This heterogeneity in composition and MRT of occluded C across soil and ecosystem types creates difficulty in developing a consistent understanding and prediction of occluded C dynamics. Models which partition organics according to structural properties can't account for the presence of a wide variety of compounds within a single functional pool, whereas models which regard SOM pools as homogenous black boxes lack the mechanistic parameters necessary for linking shifts in environmental parameters with shifts in SOM MRT (Derrien and Amelung, 2011; Kuzyakov, 2011; Manzoni and Porporato, 2011). Thus occluded organics, though

functionally very different than other pools of SOM, are not represented accurately in current modelling efforts.

In order to gain a better understanding of the mechanisms regulating occluded SOM genesis and turnover in forest soils, we density separated soils from a lithosequence under *P. ponderosa*. The use of a lithosequence under a single vegetation type was used to examine the specific influence of mineral assemblage on occluded fraction characteristics while constraining other highly influential soil forming factors such as climate and plant inputs. Four parent materials were examined (dolostone, basalt, granite, and rhyolite) that encompass a wide range of soil texture, mineral assemblage, and acidity (Heckman and Rasmussen, 2011). Samples from each genetic horizon were density separated, and isolated fractions were examined using a combination of ^{13}C, ^{15}N, total organic C and N, ^{14}C abundance, pyrolysis gas chromatography/mass spectrometry (GC/MS), and cross polarization magic angle spinning (CPMAS) ^{13}C nuclear magnetic resonance (NMR) spectrometry. We sought to define the major controls on the composition and MRT of occluded SOM with specific focus on the following questions: i) How is the occluded fraction distinguishable from organics associated with mineral surfaces (mineral fraction) and organics neither associated with mineral surfaces nor occluded within aggregates (free/light fraction)? ii) What is the influence of soil aggregate stability on occluded SOM composition and MRT? and iii) How does the occluded fraction vary in MRT and composition both with changes in depth and among soils of differing mineral assemblage? We hypothesized that mineral assemblage would exert significant control over occluded SOM composition and MRT indirectly through its influence on aggregate stability and turnover rates. We also hypothesized that occluded SOM composition and MRT would

shift significantly with depth in the profile, following variation in the composition and lability of plant inputs.

2. Methods

2.1 Sample sites & soil physiochemical properties

Sample site characteristics and soil mineral assemblages are discussed in detail in Heckman and Rasmussen (2011). Briefly, three replicate soil pedons were sampled in Arizona, USA, from a lithosequence comprising four different parent materials: rhyolitic ash, granite, basalt, and dolostone. Soils from the dolostone site were developed from dual parent materials: the underlying dolomitic dolostone bedrock and mafic ash deposited during the formation of nearby cinder cones. Climate and vegetation characteristics were nearly equivalent among sites, so that differences in soil and organic matter characteristics can reasonably be attributed to differences in parent material characteristics. All soils were sampled from north-facing backslope positions with *Pinus ponderosa* as the dominant canopy species. Mean annual temperature ranged from 9-12°C. Mean annual precipitation ranged from 675-815 mm yr^{-1}. Previously measured soil characteristics including soil texture, specific surface area, quantitative mineral composition, pH, EC, and exchangeable cations were used in correlation analyses in the current study. These mineral and physiochemical characteristics and methods are given in Heckman and Rasmussen (2011).

2.2 Density separation, elemental & isotope analysis

Soils from each horizon of all three replicate pedons of each parent material were density separated at 1.8 g cm^{-3}, following the methods of Rasmussen et al. (2005).

Briefly, the free/light fraction was floated off after mixing 30 g bulk soil with 150 cm^{-3} of a sodium polytungstate solution adjusted to a density of 1.8 g cm^{-3}. Soils were then subjected to sonication a rate of 1500 J g^{-1} soil in order to disrupt aggregates and liberate occluded organics. Following sonication, the occluded fraction was floated off. Losses of mass, C, and N during density separation are given in Supplementary table 1.

Samples were analyzed for %C, %N, $\delta^{13}C$, and $\delta^{15}N$ by dry combustion at 1000°C with an elemental analyzer (Costech Analytical Technologies, Valencia, CA, USA) coupled to a continuous-flow mass spectrometer (Finnigan Delta PlusXL, San Jose, CA, USA) at the University of Arizona Stable Isotope Laboratory.

Radiocarbon abundance of the density/aggregate fractions and bulk soils was measured by Accelerator Mass Spectrometry (AMS) at the NSF - Arizona AMS Laboratory at the University of Arizona (Tucson, AZ) (Donahue et al., 1990), the Centro Nacional de Aceleradores (Seville, Spain) (Arévalo et al., 2009), and the Center for AMS at Lawrence Livermore National Laboratory (Livermore, CA) (Vogel et al., 1987; Davis et al., 1990). For each horizon, density/aggregate fractions and bulk soils from each site were composited for AMS analysis.

2.3 CP/MAS ^{13}C-NMR analysis

For the NMR spectroscopic analysis, composite samples were obtained from all three pedons sampled at each site, yielding one composite sample per genetic horizon. Prior to NMR analysis, bulk soil samples were treated four times with 10% hydrofluoric acid (HF) to remove iron oxides and concentrate the organic fraction following Gonçalves *et al.* (2003). Mass, C, and N recovery percentages of soils following HF digestion are given in Supplementary table 2. In addition the occluded C fraction of each genetic horizon was analyzed.

The ^{13}C NMR spectra were acquired with a Bruker DSX 200 spectrometer operating at a ^{13}C resonance frequency of 50.32 MHz. Samples were confined in a zirconium oxide rotor with an external diameter of 7 mm. The variable amplitude cross polarization magic angle spinning technique was applied with a contact time of 1 ms, a spinning speed of 6.8 kHz and a pulse delay of 1 s. For quantification, the spectra were subdivided into different chemical shift regions according to Fründ and Lüdemann (1989, 1991) and Knicker and Lüdemann (1995), and spinning side band corrections were applied (Knicker et al. 2005). The relative intensity distribution of ^{13}C was determined by integrating the signal intensity in different chemical shift regions with an integration routine supplied with the instrument software. From these data, the degree of aromaticity (%) was calculated (Hatcher et al. 1981), as well as the ratio of alkyl to *O*-alkyl C, as an indicator of the degree of OM decomposition (Baldock et al. 1997). Studies have shown that NMR spectroscopy has good reproducibility, with a standard deviation of <10% for the relative intensities determined for the various chemical shift regions (Dieckow et al. 2005; Knicker, 2011).

2.4 Pyrolysis Gas Chromatography/Mass Spectrometry (Py GC/MS)

To achieve a more detailed molecular characterization of the samples, selected density/aggregate fractions and bulk soil samples were analyzed by pyrolysis GC/MS. Selected subsurface density/aggregate fractions were analyzed at the Biogeochemistry and Nutrient Cycling Lab at the University of California, Davis. Samples were pyrolyzed at 590°C in pyrofoils (Pyrofoil F590, Dychrom, Sunnyvale, CA) within a Curie Point pyrolyzer (Japan Analytical Industry Co.) following methods detailed in Throckmorton (2012).

187 Selected surface density/aggregate fractions were analyzed at the Institute of
188 Natural Resources and Agrobiology, National Research Council, in Seville, Spain.
189 Samples were pyrolyzed 500°C (pyrolyzer model 2020, Frontier Laboratories Ltd.
190 Fukushima, Japan) in platinum cups. Detailed experimental conditions are given in the
191 supplementary methods.
192 Pyrolysis products were identified through peak comparison with published and
193 stored (NIST and Wiley libraries) data. The sum of all identified pyrolysis products'
194 total ion signal integrated area was defined as 100%, from which the relative amount of
195 each pyrolysis product was calculated. Results were expressed as the relative abundance
196 of total identifiable compounds and grouped into 7 chemical classes: benzene, lignin,
197 lipid, phenol, polysaccharide, and nitrogenous.
198
199 ***2.5 Aggregate stability***
200 Aggregate abundance and stability was measured by horizon for each pedon,
201 following procedures modified from Fuller and Goh (1992), Rasmussen et al. (2005),
202 and White et al., (2009). This method of measuring aggregate stability uses the amount
203 of clay released per unit of energy applied as a metric of aggregate disruption and
204 assumes that the greater the amount of clay measured in a sonicated sample corresponds
205 to the amount of aggregates that were broken apart. Aggregate stability then is
206 negatively correlated with clay release. Data analysis followed Rasmussen et al. (2005).
207 Briefly, a four parameter exponential growth model was fitted to plots of energy (J)
208 versus clay release (% relative to clay release at 1500 J):
209 $\%\ clay\ released = a\left(1 - e^{-b(J(g\ soil)^{-1}}\right) + c\left(1 - e^{-d(J(g\ soil)^{-1}}\right)$,
210 where a and c represent pool sizes in units % clay released, b and d are constants for
211 each pool in units of $[J(g\ soil)^{-1}]^{-1}$. The stability of the aggregate pool was estimated by

212 the inverse of the exponential constant, estimating the Joules per gram of soil required
213 to disaggregate the aggregate structures in that pool. Model parameters were fitted by a
214 least squares regression technique (Raine and So, 1993).
215
216 ***2.6 Data and statistical analyses***
217 The Molecular Mixing Model published by Nelson and Baldock (2005) was
218 applied to the NMR data. This model uses ratios of peak areas from NMR spectra to
219 estimate the relative abundance of organic compound classes in the sample. Organic
220 compound classes included: carbohydrate, nitrogenous compounds, lignin, aliphatic
221 material, carbonyl, and charcoal.
222 Mean residence times (MRT) of bulk soils and density/aggregate fractions were
223 calculated using the measured radiocarbon abundance and a time-dependent steady-state
224 model (Trumbore 1993; Torn et al. 2002). This model assumes all new organic inputs to
225 each modeled fraction bear an atmospheric radiocarbon signature and does not account
226 for lag times associated with the transfer of organics among fractions, so calculations
227 likely overestimate MRTs. Due to the incorporation of "bomb" radiocarbon into soil
228 fractions at different rates, some fractions had two possible MRTs. In all cases where
229 two MRT solutions were possible, the shorter MRT was eliminated as a possible
230 solution due the unreasonably large predicted yearly output of C from the fraction
231 (>30% of total pool respired per year).
232 A total of three replicate pedons were sampled per study site. Significant
233 differences between density/aggregate fraction characteristics across sites were
234 determined by one-way ANOVA followed by Tukey-Kramer *post hoc* test at a 95%
235 confidence limit (n=3 for each site). Simple linear least-squares regression and multiple
236 linear regression were used to examine relationships between soil physicochemical

variables, aggregate stability, estimated MRTs, and occluded SOM properties (n=14). Principal components analysis (PCA) of the compound classes was used to succinctly illustrate variance in Py GC/MS data across sites. To avoid issues of colinearity, explanatory variables with correlation coefficients greater than 0.70 were not concurrently included in regression models (Zar, 1999).

3. Results

3.1 Elemental data ($\delta^{13}C$, $\delta^{15}N$, C-to-N, ^{14}C)

Elemental composition differed significantly among density fractions (Table1). C-to-N ratios, ^{13}C enrichment, and ^{15}N enrichment were similar among free/light and occluded fractions. Mineral fractions had significantly lower C-to-N ratios and were enriched in both ^{13}C and ^{15}N in comparison to both free/light and occluded fractions. Occluded fraction elemental composition did not differ significantly among mineral assemblages, but did vary with depth (Table 2). The occluded fraction accounted for the smallest total amount of C among the three fractions (Figure 1), and its relative abundance generally decreased with depth. Relative abundance of occluded C was highest in surface horizons of the dolostone and basalt soils (~30%), and lowest at the soil/saprolite boundary of the rhyolite, granite and basalt soils (~10%).

The modeled MRT of the occluded fraction generally increased with depth and was longer than any other fraction of SOM in all but the BCr horizon of the rhyolite soils. In the deeper soils, rhyolite and basalt, the occluded fraction decreased in MRT at the soil/saprolite boundary. The free/light fraction consistently had the shortest MRT of all the fractions, and varied little with depth. Mineral/heavy fractions generally had MRTs intermediate between free/light and occluded fractions (Figure 2, Table 2).

Detailed data associated with radiocarbon measurements is given in Supplementary Table 3.

3.2 *^{13}C CPMAS-NMR* spectroscopy

Due to the analysis time and cost associated with NMR analyses, only bulk SOM and occluded fractions were examined by NMR spectroscopy. *O*-alkyl/alkyl ratios increased with depth in both the occluded and bulk SOM, an indication of increasing degree of decomposition with depth (Baldock et al., 1997). A comparison of the occluded to the bulk SOM across all soils revealed consistent and significant differences. Bulk SOM had a significantly higher concentration of proteins (P = 0.0082), lignin (P = 0.0120), and carbohydrates (0.0038) than the occluded SOM. However, the most striking difference between bulk SOM and occluded SOM was the large enrichment of charcoal in the occluded fractions (P = 0.0099). High intensity in the chemical shift region between 140 and 110 ppm is indicative of charcoal content (Supplementary figure 1), especially when it is unaccompanied by low intensity in the 140-160 ppm range. Both the Molecular Mixing Model (Nelson and Baldock, 2005) and the *C-H*-aryl *C/O*-aryl intensity ratio (Dieckow et al., 2005) were used as metrics of charcoal content (Table 3), and the two estimates of charcoal content were highly correlated (r^2 = 0.80, P < 0.0001). The occluded fraction was significantly enriched in charcoal in comparison to bulk SOM at all depths and in all soils, regardless of mineral assemblage, though the absolute charcoal content of the occluded fraction tended to decrease in the deepest horizons (Figure 3).

Comparison of SOM molecular composition on the basis of soil parent material type was confounded by differences in depth among the soils and the lack of replication (only composite samples were analyzed). However, qualitative examination of the

NMR spectra revealed both similarities and differences among soils (Supplementary figure 1). Bulk SOM was similar in molecular composition among soils aside from a large enrichment in aliphatic C (alkyl peak, 0-45 ppm) in the surface of the granite soil. Occluded SOM appeared to vary both with depth and among soils. In the rhyolite soils occluded fraction charcoal content was highest in the surface horizon and decreased with depth, whereas the opposite trend was observed in the basalt soils. The occluded fraction of the granite surface soil showed the same enrichment in aliphatic C as the granite bulk SOM.

3.3 Pyrolysis GC/MS

Composition of free/light, occluded, and mineral/heavy OM fractions are easily distinguished from one another based on pyrolysate abundance. Most notably, the mineral/heavy fraction was enriched in nitrogenous compounds and depleted in lignin and lipids relative to the free/light and occluded fraction (Table 1). Other significant differences among fractions included enrichment of lipids and benzenes in the free/light fraction, and enrichment of phenol-based pyrolysates in the occluded fraction. Free/light and occluded fractions were similar among parent materials, but the mineral/heavy OM fractions show substantial variation among parent materials (Figure 4a, Table 2). Variation in occluded fraction molecular composition followed variation in bulk C composition (Table 4).

Figure 4a shows a PCA plot of compound class abundance (benzene, phenol, lignin, polysaccharide, and nitrogenous) for each fraction from the two soil horizons (surface versus subsurface) analyzed for each soil parent material. Samples grouped according to fraction type (free/light, occluded, mineral) along principal component axis 1 (accounting for 44% of total variance), and grouped according to depth along

311 principal components axis 2 (accounting for 27% of total variance). Regression of
312 compound class data against the principal component values indicated that nitrogenous
313 compound content accounted for the bulk of the variation in samples along axis 1 (r^2 =
314 0.77, $p < 0.0001$), with nitrogenous compound content increasing from right to left along
315 the axis. Benzene and phenol abundance accounted for variance along axis 2 ($r^2 = 0.87$,
316 $p < 0.0001$). Within occluded fractions (Figure 4b), surface and subsurface samples
317 differed based on lignin, polysaccharide, and phenol content. Principal components axis
318 1 accounted for 37% of total variance. Principal components axis 2 accounted for 26%
319 of total variance.
320
321 ***3.4 Aggregate stability***
322 Aggregate stability analyses excluded the rhyolite BCr and granite AC horizons
323 due to the abundance of saprolitic materials in these horizons. Aggregate stability did
324 not vary consistently among the soils or mineral assemblages examined, but did show
325 relationships with soil % clay and depth (Table 5). Abundance of weak aggregates
326 increased with depth and strong aggregate abundance decreased with depth in all soils
327 except those derived from granite, likely driven by organic matter content (strength of
328 aggregates estimates based on the amount of energy required for disruption). Increasing
329 clay content increased the abundance of weak aggregates, but decreased the abundance
330 and stability of strong aggregates. Weak aggregates decreased in strength with depth in
331 all soils, likely due to the lower abundance of organics at depth.
332
333 ***3.5 Correlation analysis***
334 A simple statistical exploration of the NMR data revealed that after accounting
335 for the influence of depth, both indices of occluded SOM charcoal content (modeled %

char and (C-, H-aryl)/O-aryl ratio) were strongly positively correlated with occluded C MRT (depth + % char: $r^2 = 0.85$, $p < 0.0001$; depth + (C-, H-aryl)/O-aryl: $r^2 = 0.77$, $P = 0.0002$). Depth and charcoal content accounted for similar amounts of variation in occluded SOM MRT. Bulk SOM MRT was not significantly correlated with charcoal content. Though the MRT of both the bulk and occluded SOM showed variance among soils, they did not vary predictably according to soil parent material. Bulk SOM MRT was highly correlated with depth ($r^2 = 0.63$, $P = 0.0004$), but occluded MRT was not ($r^2 = 0.21$, $P = 0.085$). Neither occluded C abundance nor MRT were correlated with aggregate stability after accounting for the influence of depth.

4. Discussion

The most notable quality of the occluded fraction was the selective preservation of pyrogenic materials. The high intensity of the signal at around 130 ppm in the ^{13}C NMR spectra, the elevated C-to-N ratio and the high concentration of benzene- and phenol-containing compounds noted in the pyrolysis GC/MS data all support a large polyaromatic content in occluded fractions in comparison to bulk soil and other density fractions. The enrichment of charcoal in occluded fractions in comparison to bulk soils was present in all soils regardless of mineral assemblage and generally increased with depth, reaching nearly five times the concentration of charcoal in the subsurface of the basalt soil (Fig 3a). This same trend has been observed by other authors (Skjemstad et al., 1992) and most notably by Brodowski (2006). Stable isotope enrichment levels suggested a similar degree of decomposition among free/light and occluded fractions, while elemental data and molecular structure data indicate mineral/heavy fractions were substantially more processed, and bore a microbial signature in comparison to the more plant-like character of free/light and occluded fractions (Baisden et al., 2002).

Occluded C characteristics changed consistently with depth, generally corresponding to changes in free/light and bulk SOM characteristics, suggesting that relatively undecomposed particulate organic matter is occluded within aggregates during their formation and turnover. The fact that occluded C MRT increased with depth, while free/light C did not may indicate a mostly one-way flow of organics from the free/light to occluded fraction in these soils and may additionally suggest that aggregate turnover at depth operates at timescales reaching or exceeding thousands of years. If this is indeed the case, it lends new insight into the modeling of SOM transfer among distinct SOM pools. The occluded fraction is often assumed to be intermediate in degree of decomposition and stability between the free/light and mineral/heavy fractions (von Lützow et al., 2007), with active transport among all three fractions but most notably between free/light and occluded fractions as aggregates disassociate and reform as soils weather and experience seasonal climatic changes (Kelly et al., 1997). However a clear understanding of the links and fluxes between SOM pools is still mostly lacking (Kuzyakov, 2011), and the identification of a relatively passive and chemically distinct occluded particulate fraction in western U.S. conifer forest soils may help clarify the direction and magnitude of between-pool fluxes in these systems.

Contrary to our hypotheses, occluded SOM characteristics were not linked to variance in soil mineral assemblage or aggregate abundance/stability. If turnover of occluded C was dependent on the dissolution and reformation of aggregates, occluded C MRT should show a correlation with aggregate stability/turnover. The lack of correlation among aggregate stability parameters and occluded C characteristics indicates that either aggregate stability is not a good predictor of occluded C protection against biodegradation or the laboratory methods employed here to gauge aggregate stability are not a good proxy for aggregate turnover under field conditions. It's likely

that application of sonic energy to disrupt aggregate structures does not mimic the natural processes governing aggregate dissolution and reformation such as wet/dry cycles, clay flocculation, and root/mycelium growth. It may also be that the actual bond strength among aggregate components is less important than the amount of disturbance a particular soil horizon experiences, and weakly bonded aggregates may persist at depth but experience high turnover in surface horizons. The lack of relationships among aggregate parameters, mineral assemblage and occluded fraction abundance and MRT suggest that persistence of occluded organics in these soils is not strongly dependent on the presence of specific mineral phases, soil texture, or the aggregation qualities associated with specific clay types/abundance.

We hypothesized that aggregate stability would vary considerably and consistently among soils of differing mineral assemblage, with oxyhydroxide phases and 1:1 phyllosilicate content driving increases in aggregate abundance and stability (Six et al., 2002). Correlation analysis indicated that aggregate stability and abundance had significant relationships only among percent clay and depth. Increasing depth was associated with a decrease in the stability of weaker aggregates, perhaps due to a decrease in organic coatings on mineral surfaces and a lower level of biological activity. This explanation is consistent with previous research indicating a strong dependence of microaggregate stability on organic binding agents in a variety of soils (Tisdall and Oades, 1982; Amézketa, 1999). Increases in clay content had an inconsistent effect on aggregate parameters, increasing the abundance of weak aggregates but decreasing the abundance and stability of stronger aggregates. This is possibly due to the relative abundance of illite and vermiculite clays in these soils, phases which render aggregates most sensitive to dispersion (Amézketa, 1999 and references therein). The abundance of Fe and Al oxyhydroxide phases is often implicated in driving a large amount of

411 variation in SOM turnover (Torn et al., 1997; Parfitt et al., 2002), but did not show a
412 relationship with occluded C MRT in these soils. Likewise, oxyhydroxides did not
413 account for any variation in aggregate parameters. However this may be due to the
414 relatively low abundance of oxyhydroxides in the majority of the soils examined in this
415 study.

416 Charcoal content of the occluded fraction was highly correlated with both the
417 abundance and MRT of C in this fraction, indicating that fire exerts a large degree of
418 control over the formation and preservation of occluded organics in soils of temperate
419 forests that include wildfire as a component of ecosystem processes. A compilation of
420 available data from forested systems (including the data from this study) indicates
421 significant variation in occluded fraction MRT depending upon wildfire regime (Fig. 5).
422 Specifically, data from western U.S. (Arizona and California) conifer forests prone to
423 burning (Rasmussen et al., 2005; Heckman et al., 2009; Lybrand et al., 2013) indicates
424 that the occluded C tends to be the oldest fraction of soil C (Fig. 2, Fig. 5a) with mean
425 residences times generally twice that of the bulk soil (Fig. 5c). In contrast, wet forested
426 ecosystems (McFarlane et al., 2012; Marin-Spiotta et al., 2008) exhibit little variation in
427 radiocarbon content among free light, occluded, and mineral fractions (Fig 5b), with
428 occluded C MRT roughly equivalent to that of the bulk C (Fig. 5d). Thus, differences in
429 fire regime may partially account for the high degree of heterogeneity in occluded
430 fraction composition and MRT among forested ecosystems.

431 The physiochemical properties of charcoal are a probable mechanism to explain
432 the preservation of occluded C in these systems, due both to the inherent structural
433 recalcitrance of pyrogenic materials and the reactivity of charcoal structures (Schmidt
434 and Noack, 2000; Brodowski et al., 2005, 2006; Czimczik and Masiello, 2007;
435 Keiluweit and Kleber, 2009; Knicker 2011). Condensed polyaromatic structures are

436 metabolically unfavorable in comparison to other microbial growth substrates, and the
437 strongly sorbing aromatic π-systems of charcoal can form strong bonds with other soil
438 constituents (Keiluweit and Kleber, 2009), properties long recognized to promote the
439 long-term preservation of charcoal in soils. The hydrophobicity of charcoal surfaces
440 also plays a role in its preservation though reducing wettability which effectively limits
441 enzymatic access. Hydrophobic organic domains also promote strong interactions with
442 phyllosilicates, especially kaolinite (Puget et al., 2000; Bachmann et al., 2008;
443 Ellerbrock et al., 2005). How much of a part the actual formation of soil aggregates
444 plays in protecting these organics from biodegradation isn't clear, but radiocarbon-
445 based MRT estimates indicate occlusion within aggregates or coating of occluded OM
446 surfaces with mineral particles does contribute significantly to the persistence of these
447 organics (Wagai et al., 2009). This observation is additionally supported by the
448 comparatively fast turnover and lack of charcoal observed in the free/light fractions of
449 these soils, and previous research describing rapid mineralization of unprotected
450 charcoal (Marschner et al., 2008; Hilscher and Knicker, 2011). It can be said that fire is
451 the origin of a large fraction of occluded C in these soils, and the molecular properties
452 of the pyrogenic materials promote their occlusion within aggregates.
453 Though the occluded fraction contained the least amount of C relative to
454 free/light and mineral/heavy fractions, it generally had the longest MRT in soils
455 regardless of mineral assemblage indicating that this fraction is an important repository
456 of stable C in western U.S. conifer forest soils. In forested soils which experience
457 periodic fire events, it appears that it is only through the combination of chemical
458 recalcitrance and occlusion within aggregates that organics can attain "passive" MRTs.
459 Additionally, these results indicate that fire regime may be a good indicator of the
460 abundance of the passive C fraction in temperate forest soils, though how charcoal

degradation rates will be modified by changes in climate has not been resolved (Liski et al., 1999; Nguyen et al., 2010).

4.1 Conclusions

Data describing the molecular composition of occluded organics in these soils indicated that the fraction is dominated by pyrogenic materials regardless of the particular soil mineral assemblage or estimated aggregate stability. Radiocarbon-based MRTs of occluded organics revealed that occluded C has a greater resistance to biodegradation than C stabilized through bonding to mineral surfaces (mineral/heavy fraction), and that this stabilization can be directly linked to the abundance of charcoal in the occluded fraction. Results point to the importance of fire as a driver of occluded C formation, and the structural recalcitrance of pyrogenic materials as a major mechanism of occluded C stabilization in these systems. These findings suggest that understanding the fire regime of temperate forest ecosystems may be important in modeling the abundance and behavior of passive SOM pools.

Acknowledgments

This work was funded by a grant from the National Science Foundation to S. Brantley and T. White (EAR #0725019), a grant from the National Science Foundation to C. Rasmussen, J. Chorover and E. Schwartz (DEB #0543130), a grant from the National Science Foundation to C. Rasmussen and M. Schaap (EAR/IF # 0929850), and a graduate student research grant from the Geological Society of America. The authors wish to thank Trinidad Verdejo for her assistance in obtaining and analyzing pyrolysis GC/MS data at IRNAS, and Dr. S. Mercer Meding for his support and assistance at the University of Arizona. A portion of the radiocarbon data included in this manuscript

was generously provided by the Radiocarbon Collaborative, which is jointly sponsored by the USDA Forest Service, Lawrence Livermore National Laboratory and Michigan Technological University. We acknowledge support from the J. G. Boswell Endowed Chair in Soil Science for supporting the pyrolysis GC/MS analysis. A portion of this work was performed under the auspices of the U.S. Department of Energy by Lawrence Livermore National Laboratory under contract DE-AC52-07NA27344, LLNL-JRNL-646432. We also wish to acknowledge the insights and efforts of two anonymous reviewers who helped improve the quality of this manuscript.

References:

Amézketa, E., 1999. Soil aggregate stability: A review. Journal of Sustainable Agriculture 14, 83-151.

Arévalo, F.J.S., Martínez, I.G., León, M.G., 2009. Radiocarbon measurement program at the Centro Nacional de Aceleradores (CAN), Spain. Radiocarbon 51, 883-889.

Baisden, W.T., Amundson, R., Cook, A.C. Brenner D.L.,2002. Turnover and storage of C and N in five density fractions from California annual grassland surface soils. Global Biogeochemical Cycles 16, 117-132.

Bachmann, J., Guggenberger, G., Baumgartl, T., Ellerbrock, R.H., Urbanek, E., Goebel, M.-O., Kaiser K., Horn, R., Fischer, W.R., 2008. Physical carbon-sequestration mechanisms under special consideration of soil wettability. Journal of Plant Nutrition and Soil Science 171, 14-26.

Baldock, J.A., Oades, J.M., Nelson, P.N., Skene, T.M., Golchin, A., Clarke, P., 1997. Assessing the extent of decomposition of natural organic materials using solid state ^{13}C NMR spectroscopy. Australian Journal of Soil Research 35, 1061–1083.

Brodowski, S., Amelung, W., Haumaier, L., Abetz, C., Zech, W., 2005. Morphological and chemical properties of black carbon in physical soil fractions as revealed by scanning electron microscopy and energy-dispersive X-ray spectroscopy. Geoderma 128, 166-126.

519

520 Brodowski, S., John, B., Flessa, H., Amelung, W., 2006. Aggregate-occluded black
521 carbon in soil. European Journal of Soil Science 57, 539-546.

522

523 Crow, S., Swanston, C.W., Lajtha, K., Brooks, R., Keirstead, H., 2007. Density
524 fractionation of forest soils: methodological question and interpretation of incubation
525 results and turnover time in an ecosystem context. Biogeochemistry 85, 69-90.

526

527 Czimczik C.I., Masiello C.A., 2007. Controls on black carbon storage in soils. Global
528 Biogeochemical Cycles 21, DOI: 10.1029/2006GB002798.

529

530 Davis J.C., Proctor, I.D., Southon, J.R., Caffee, M.W., Heikkinen, D.W., Roberts, M.L.,
531 Moore, T.L., Turteltaub, K.W., Nelson, D.E., Loyd, D.H., Vogel, J.S., 1990. LLNL/US
532 AMS facility and research program. Nuclear Instruments and Methods in Physics
533 Research, Sect. B 52, 269-272.

534

535 Derrien, D., Amelung, W., 2011. Computing the mean residence time of soil carbon
536 fractions using stable isotopes: impacts of the model framework. European Journal of
537 Soil Science 62, 237-252.

538

539 Dieckow, J., Mielniczuk, J., Knicker, H., Bayer, C., Dick, P.D., Kögel-Knabner, I.,
540 2005. Composition of organic matter in a subtropical Acrisol as influenced by land use,
541 cropping and N fertilization, assessed by CPMAS ^{13}C NMR spectroscopy. European
542 Journal of Soil Science 56, 705–715.

543

Donahue, D.J., Jull, A.J.T., Toolin, L.J., 1990. Radiocarbon measurements at the University of Arizona AMS facility. Nuclear Instruments and Methods in Physics Research Section B: Beam Interactions with Materials and Atoms 52, 224-228.

Ellerbrock, R.H., Gerke, H.H., Bachmann, J., Goebel, M.O., 2005. Composition of organic matter fractions for explaining wettability of three forest soils. Soil Science Society of America Journal 69, 57-66.

Fuller, L.G., Goh, T.B., 1992. Stability-energy relationships and their application to aggregation studies. Canadian Journal of Soil Science 72, 453-466.

Fründ, R., Lüdemann, H.-D., 1989. The quantitative analysis of solution and CPMAS-C-13 NMR spectra of humic material. Science of the Total Environment 81/82, 157 168.

Fründ, R., Lüdemann, H.-D., 1991. Quantitative characterization of soil organic matter and its fractionation products by solid state high resolution C-13 (CPMAS) Spectroscopy. Zeitschrift für Naturforschung 46c, 982-988.

Golchin, A., Oades, J.M., Skjemstad, J.O. and Clarke, P., 1994. Study of free and occluded particulate organic-matter in soils by solid-state ^{13}C CP/MAS NMR-spectroscopy and scanning electron-microscopy. Australian Journal of Soil Research 32, 285–309.

568 Gonçalves, C.N., Dalmolin, R.S.D., Dick, D.P., Knicker, H., Klamt, E., Kögel-Knabner,
569 I., 2003. The effect of 10% HF treatment on the resolution of CPMAS ^{13}C NMR spectra
570 and on the quality of organic matter in Ferralsols. Geoderma 116, 373-392.
571
572 Hatcher, P.G., Schnitzer, M., Dennis, L.W., Maciel, G.E., 1981. Aromaticity of humic
573 substances in soils. Soil Science Society of America Journal 45, 1089–1094.
574
575 Heckman, K.A., Rasmussen, C., 2011. Lithologic controls on regolith weathering and
576 mass flux in forested ecosystems of the southwestern USA. Geoderma 164, 99-111.
577
578 Hilscher, A., Knicker, H., 2011. Degradation of grass-derived pyrogenic organic
579 material, transport of the residues within a soil column and distribution in soil organic
580 matter fractions during a 28 month microcosm experiment. Organic Geochemistry 42,
581 42-54.
582
583 Jackson, M.L., 1985. Soil Chemical Analysis: Advanced Course, revised second ed.
584 Paralled Press University of Wisconsin-Madison Libraries, Wisconsin.
585
586 Keiluweit, M., Kleber, M., 2009. Molecular-level interactions in soils and sediments:
587 the role of aromatic π-systems. Environmental Science and Technology 43, 3421-3429.
588
589 Kelly, R.H., Parton, W.J., Crocker, G.J., Grace, P.R., Klír, J., Körschens, M., Poulton,
590 P.R., Richter, D.D., 1997. Simulating trends in soil organic carbon in long-term
591 experiments using the century model. Geoderma 81, 75-90.
592

Kögel-Knabner, I., Kleber, M., 2011. Mineralogical, Physiochemical, and Microbiological Controls on Soil Organic Matter Stabilization and Turnover. In: Huang, P.M., Li, Y., Sumner, M.E. (Eds.), Handbook of Soil Sciences: Resource Management and Environmental Impacts, second ed. CRC Press, Florida, pp. 7.1-7.22

Knicker, H., Lüdemann, H-D., 1995. ^{15}N and ^{13}C CPMAS and solution NMR studies of ^{15}N enriched plant material during 600 days of microbial degradation. Organic Geochemistry 23, 329–341.

Knicker, H., Saggar, S., Bäumler, R., McIntosh, P.D. and Kögel-Knabner, I.: Soil organic matter transformations induced by *Hieracium pilosella* L. in tussock grassland of New Zealand, Biol. Fert. Soils, 32**,** 194–201, 2000.

Knicker, H., González-Vila, F.J., Polvillo, O., González-Pérez, J.A., Almendros, G., 2005. Fire-induced transformation of C- and N-forms in different organic soil fractions from a Dystric Cambisol under a Mediterranean pine forest (*Pinus pinaster*). Soil Biology & Biochemistry 37, 701–718.

Knicker, H., 2011. Pyrogenic organic matter in soil: Its origin and occurrence, its chemistry and survival in soil environments. Quaternary International 243, 251-263.

Kuzyakov, Y., 2011. How to link soil C pools with CO_2 fluxes? Biogeosciences 8, 1523-1537.

617 Liski, J., Ilvesniemi, H., Makela, A., Westman, C. J., 1999. CO_2 emissions from soil in
618 response to climatic warming are overestimated - The decomposition of old soil organic
619 matter is tolerant of temperature. AMBIO 28, 171–174.
620
621 Lützow, M. v., Kögel-Knabner, I., Ekschmitt, K., Matzner, E., Guggenberger, G.,
622 Marschner, B., Flessa, H., 2006. Stabilization of organic matter in temperate soils:
623 mechanisms and their relevance under different soil conditions – a review. European
624 Journal of Soil Science 57, 426 – 445.
625
626 Lützow, M. v., Kögel-Knabner, I., Ekschmitt, K., Flessa, H., Guggenberger, G.,
627 Matzner, E., Marschner, B., 2007. SOM fractionation methods: Relevance to functional
628 pools and to stabilization mechanisms. Soil Biology & Biochemistry 39, 2183-2207.
629
630 Lybrand, R., Heckman, K., Rasmussen, C., 2013. Climate and topographic controls on
631 soil organic carbon cycling in southern Arizona. Mineralogical Magazine 77, 1659-
632 1663.
633
634 Manzoni, S., Porporato, A., 2009. Soil carbon and nitrogen mineralization: Theory and
635 models across scales. Soil Biology & Biochemistry 41, 1355-1379.
636
637 Marin-Spiotta, E., Swanston, C.W., Torn, M.S., Silver, W.L., Burton, S.D., 2008.
638 Chemical and mineral control of soil carbon turnover in abandoned tropical pastures.
639 Geoderma 143, 49-62.
640

641 Marschner, B., Brodowski, S., Dreves, A., Gleixner, G., Gude, A., Grootes, P.M.,
642 Hamer, U., Heim, A., Jandl, G., Ji, R., Kaiser, K., Kalbitz, K., Kramer, C., Leinweber,
643 P., Rethemeyer, J., Schäffer, A., Schmidt, M.W.I., Schwark, L., Wiesenberg, G.L.B.,
644 2008. How relevant is recalcitrance for the stabilization of organic matter is soils?
645 Journal of Plant Nutrition and Soil Science 171, 91-110.
646
647 McFarlane, K.J., Torn, M.S., Hanson, P.J., Porras, R.C., Swanston, C.W., Callaham,
648 M.A., Guilderson, T.P., 2012. Comparison of soil organic matter dynamics at five
649 temperate deciduous forests with physical fractionation and radiocarbon measurements.
650 Biogeochemistry 112, 457-476.
651
652 Nelson, P.N., Baldock, J.A., 2005. Estimating the molecular composition of a diverse
653 range of natural organic materials from solid-state ^{13}C NMR and elemental analysis.
654 Biogeochemistry 72, 1-34.
655
656 Nguyen, B.T., Lehmann, J., Hockaday, W.C., Josheph, S., Masiello C.A., 2010.
657 Temperature sensitivity of black carbon decomposition and oxidation. Environmental
658 Science and Technology 44, 3324-3331.
659
660 North, P.F., 1976. Towards an absolute measurement of soil structural stability using
661 ultrasound. Soil Science Society of America Journal 27, 451–459.
662
663 Parfitt, R.L., Parshotam, A., Salt, G.J., 2002. Carbon turnover in two soils with
664 contrasting mineralogy under long-term maize and pasture. Australian Journal of Soil
665 Research 40, 127-136.

Puget, P., Chenu, C., Balesdent, J., 2000. Dynamics of soil organic matter associated with particle-size fractions of water-stable aggregates. European Journal of Soil Science 51, 595-605.

Raine S.R., So, H.B., 1993. An energy based parameter for the assessment of aggregate bond energy. Journal of Soil Science 44, 249-259.

Rasmussen, C., Torn, M.S., Southard, R.J., 2005. Mineral assemblage and aggregates control carbon dynamics in a California Conifer Forest. Soil Science Society of America Journal 69, 1711-1721.

Schmidt, M.W.I., Noack, A.G., 2000. Black carbon in soils and sediments: Analysis, distribution, implications and current challenges. Global Biogeochemical Cycles 14, 777-793.

Singh., N., Abiven, S., Torn, M.S., Schmidt, M.W.I., 2012. Fire-derived carbon in soil turns over on a centennial scale. Biogeosciences 9, 2847-2857.

Six, J., Callewaert, P., Lenders, S., De Gryze, S., Morris, S.J., Gregorich, E.G., Paul, E.A., Paustian, K., 2002. Measuring and understanding carbon storage in afforested soils by physical fractionation. Soil Science Society of America Journal 66, 1981-1987.

689 Sohi, S.P., Mahieu, N., Arah, J.R.M., Powlson, D.S., Madari, B. Gaunt, J.L., 2001. A
690 procedure for isolating soil organic matter fractions suitable for modeling. Soil Science
691 Society of America Journal 65, 1121–1128.
692
693 Skjemstad, J.O., Waters, A.G., Hanna, J.V., Oades, J.M., 1992. Genesis of Podzols on
694 coastal dunes in southern Queensland: IV. Nature of the organic fractions as seen by ^{13}C
695 nuclear magnetic resonance spectroscopy. Australian Journal of Soil Research 30, 667-
696 681.
697
698 Swanston, C.W., Torn, M.S., Hanson, P.J., Southon, J.R., Garten, C.T., Hanlon, E.M.,
699 Ganio, L., 2003. Initial characterization of processes of soil carbon stabilization using
700 forest stand-level radiocarbon enrichment. Geoderma 128, 52-62.
701
702 Throckmorton, H.M., 2012. Diverse microbial carbon as a source of soil organic matter.
703 Ph.D. diss., University of California, Davis,
704 http://search.proquest.com/docview/1226501923?accountid=27865 (accessed April 29,
705 2014)
706 Tisdall, J.M., Oades, J.M., 1982. Organic matter and water-stable aggregates in soils.
707 Journal of Soil Science 33, 141-163.
708
709 Torn, M.S., Trumbore, S.E., Chadwick, O.A., Vitousek, P.M., Hendricks, D.M., 1997.
710 Mineral control of soil organic carbon storage and turnover. Nature 389, 170-173.
711

712 Torn, M.S., Lapenis, A.G., Timofeev, A., Fischer, M.L., Babikov, B.V., Harden, J.W.,
713 2002. Organic carbon and carbon isotopes in modern and 100-year-old-soil archives of
714 the Russian steppe. Global Change Biology 8, 941–953.
715
716 Trumbore, S.E., 1993. Comparison of carbon dynamics in tropical and temperate soils
717 using radiocarbon measurements. Global Biogeochemical Cycles 7, 275–290.
718
719 Vogel, J.S., Southon, J.R., Nelson, D.E., 1987. Catalyst and binder effects in the use of
720 filamentous graphite for AMS. Nuclear Instruments and Methods in Physics Research
721 Sect. B 29, 50-56.
722
723 Wagai, R., Mayer, L.M., Kitayama, K., Knicker, H., 2008. Climate and parent material
724 controls on organic matter storage in surface soils: A three-pool, density-separation
725 approach. Geoderma 147, 23-33.
726
727 Wagai, R., Mayer, L.M., Kitayama, K., 2009. Nature of the “occluded” low-density
728 fraction in soil organic matter studies: A critical review. Soil Science and Plant
729 Nutrition 55, 13-25.
730
731 White, D.A., A. Welty-Benard, C. Rasmussen, Schwartz. E., 2009. Vegetation controls
732 on soil organic carbon dynamics in an arid, hyperthermic ecosystem. Geoderma 150,
733 214-223.
734
735 Zar J.H., 1999. Biostatistical Analysis. Prentice Hall, Upper Saddle River, NJ.

736 Figure 1. Distribution of organic C among occluded, free/light, and mineral/heavy
737 fractions , expressed as the percentage of bulk soil organic C contained in each fraction.
738 Bars represent the standard error of three replicates per soil type.
739
740 Figure 2. Calculated mean residence times for bulk soil organic matter and
741 density/aggregate fractions for each of the four soils examined. Each point represents
742 one sample composited from three pedons.
743
744 Figure 3. a) The percentage of charcoal in the occluded fraction divided by the
745 percentage of charcoal in the bulk soil. Charcoal was enriched in the occluded fraction
746 in comparison to bulk soil organic matter in all soils. b) The percentage of total bulk soil
747 charcoal included in the occluded fraction. Note that this graph implies that charcoal is
748 present in all density/aggregate fractions, and at depth the majority of charcoal is not in
749 the occluded fraction.
750
751 Figure 4. Principal components analyses of pyrolysis GC/MS data. a) Plot shows the
752 relationship among the molecular compositions of density/aggregate fractions. b) Plot
753 shows the relationship among occluded soil organic matter fractions from soils of
754 differing mineral assemblages. Composition of occluded fractions roughly groups
755 according to depth.
756
757 Figure 5. Radiocarbon content of free light (FLF), occluded (OCC), and mineral (MIN)
758 fractions for a mix of surface and subsurface samples for [A] western conifer forests
759 prone to wildfire (n=27) and [B] wet temperate and tropical forests (n=18). Data in [C]
760 and [D] indicate the mean residence time (MRT, years) calculated for the occluded

761 fractions relative to bulk soil for the fire prone systems and wet forest systems,
762 respectively. The dashed lines are the 1:1 line and the solid black lines are best fit
763 regressions with the intercept set equal to zero.
764
765 Supplementary Figure 1. CPMAS ^{13}C NMR spectra of occluded organic matter
766 fractions and HF-treated bulk soils.
767

Table 1. Comparison of density/aggregate fraction characteristics, C/N ratios, δ13C‰, and δ15N‰ values are the depth-weighted average across all sites (n=12). Pyrolysis GC/MS compound abundances are the average of one subsurface and one surface horizon across all sites (*n* =8). Standard errors are given in parentheses.

	Elemental data			**Pyrolysis GC/MS compound abundance (% of total)**					
Fraction	C/N	$\delta^{13}C$‰	$\delta^{15}N$‰	**benzene**	**lignin**	**lipid**	**phenol**	**polysaccharide**	**Nitrogenous**
Free/Light	44.1 (±6.7)^{A}	-24.7 (±0.3)^{B}	-0.10 (±0.54)^{A}	11.9 (1.82)^{B}	31.1 (4.3)^{A}	4.8 (1.2)^{A}	11.8 (1.8)^{AB}	33.7 (3.2)^{A}	6.4 (0.9)^{B}
Occluded	48.4 (±8.8)^{A}	-24.4 (±0.3)^{B}	0.19 (±0.50)^{A}	23.8 (1.9)^{A}	27.6 (4.6)^{A}	4.0 (1.0)^{AB}	15.5 (2.7)^{A}	21.5 (2.9)^{A}	7.6 (0.6)^{B}
Mineral/Heavy	12.2 (±1.9)^{B}	-22.2 (±0.5)^{A}	1.89 (±2.12)^{A}	25.0 (2.7)^{A}	10.2 (2.1)^{B}	0.9 (0.5)^{B}	6.3 (2.1)^{B}	25.9 (5.0)$_{A}$	30.6 (5.4)^{A}

Significance was determined using one-way ANOVA by treatment followed by Tukey's HSD *post hoc* test (α=0.05). Within each column, different letters indicate statistically significant differences among variables. (*n* =12 or *n* =8) for each fraction type.

Table 2. Average C/N ratio, $\delta^{13}C‰$, $\delta^{15}N‰$, Δ14C (‰), and modeled MRT of each fraction, by horizon for each soil. Values are the average of 3 pedons per site, except for 14C and MRT which were composite samples. Standard errors are given in parentheses (n=3).

		C/N				$\delta^{13}C‰$				$\delta^{15}N‰$			$\Delta^{14}C$ (‰)				Modeled MRT (yrs)				
Parent Material	horizon	Bulk	Free/Light	Occluded	Mineral	Bulk	Free/Light	Occluded	Mineral	Free/Light	Occluded	Mineral	Bulk	Free/Light	Occluded	Mineral	Bulk	Free/Light		Occluded	Mineral
Rhyolite	A1	18 (3)	23.4 (0.9)	27.5 (4.8)	10.9 (1.9)	-25.0 (0.3)	-25.1 (0.1)	-25.0 (0.2)	-23.5 (0.3)	-0.3 (0.5)	1.2 (0.5)	3.9 (1.0)	94	46.7	-9	66	206	167	2	370	131
	A2	18 (1)	28.0 (1.8)	37.4 (2.4)	10.5 (0.8)	-24.6 (0.1)	-24.6 (0.3)	-24.1 (0.4)	-22.9 (0.2)	1.2 (0.7)	1.0 (0.3)	3.9 (0.2)	12	-6.8	-40	33	362	356	n/a	552	203
	A3	17 (3)	31.8 (2.2)	41.3 (0.2)	8.4 (0.9)	-23.9 (0.2)	-24.9 (0.0)	-24.7 (0.2)	-22.7 (0.2)	1.1 (0.7)	0.8 (0.3)	4.4 (0.1)	-12	17.9	-107	24	416	251	n/a	1099	231
	B_w1	14 (1)	35.1 (2.3)	31.2 (3.9)	21.1 (10.5)	-23.7 (0.3)	-25.4 (0.1)	-24.6 (0.0)	-23.0 (0.3)	1.2 (0.4)	1.4 (0.5)	-0.7 (1.1)	-53	40	-101	-72	628	186	n/a	1040	785
	B_w2	13 (2)	36.9 (2.6)	31.6 (1.0)	18.0 (9.0)	-23.3 (0.3)	-25.3 (0.2)	-24.7 (0.1)	-22.5 (0.2)	0.9 (0.5)	1.6 (0.3)	1.0 (2.7)	-71	59.8	-106	-39	445	140	4.5	1085	545
	BC_r	11 (1)	41.2 (3.7)	26.3 (6.6)	11.0 (3.5)	-23.1 (0.1)	-25.2 (0.1)	-24.9 (0.0)	-22.2 (0.1)	-0.3 (0.4)	1.1 (0.2)	0.2 (5.7)	-78	79.0	-44	-133	959	109	7.4	583	1346
Granite	A1	20 (1)	33.9 (3.3)	44.8 (5.0)	14.7 (0.3)	-24.4 (0.1)	-25.0 (0.1)	-24.9 (0.2)	-23.9 (0.1)	-1.5 (1.0)	-0.7 (0.7)	-0.7 (1.8)	60	100.4	16	80	116	83	10	259	109
	A2	17.3 (1)	40.6 (4.6)	51.7 (6.8)	10.4 (0.7)	-23.9 (0.1)	-25.0 (0.2)	-24.4 (0.0)	-23.5 (0.2)	0.5 (1.1)	-0.6 (0.9)	1.3 (2.5)	29	44.1	-30	56	218	173	2	489	148
	AC	19 (1)	47.8 (9.2)	62.0 (8.3)	14.5 (1.1)	-23.8 (0.1)	-24.4 (0.4)	-24.8 (0.2)	-22.9 (0.2)	-0.7 (0.7)	-0.3 (0.8)	-4.5 (5.5)	35	65	-46	28	201	131	5	593	219
Basalt	A	19 (<1)	36.8 (2.2)	43.8 (1.3)	11.6 (0.8)	-24.0 (<0.1)	-24.9 (0.1)	-24.5 (0.1)	-22.7 (0.1)	-1.6 (0.7)	-0.4 (0.8)	2.4 (0.2)	66	91.3	40	75	133	93	9	185	116
	B_t1	16 (2)	48.6 (8.2)	60.1 (5.4)	9.6 (1.5)	-22.7 (0.4)	-24.3 (0.4)	-24.0 (0.1)	-21.6 (0.3)	0.4 (0.1)	0.5 (1.0)	5.6 (1.0)	27	80.2	-50	-5	353	107	7.6	619	349
	B_t2	13 (<1)	69.3 (4.7)	83.4 (0.6)	10.7 (0.6)	-21.9 (0.2)	-24.1 (0.2)	-23.7 (0.3)	-21.0 (0.1)	0.8 (0.5)	1.7 (0.4)	2.6 (2.3)	-76	104	-268	-131	1270	82	11	3018	1326
	B_t3	12 (<1)	69.3 (1.0)	81.9 (10.5)	9.9 (2.7)	-21.7 (0.3)	-24.2 (0.2)	-23.9 (0.1)	-23.8 (2.6)	-0.6 (0.6)	-1.5 (0.7)	4.4 (3.4)	-143	43.7	-235	-203	1808	174	1.5	2549	2131
Dolostone	A	20 (2)	33.7 (3.8)	38.7 (0.8)	14.2 (1.7)	-23.0 (0.6)	-24.4 (0.5)	-24.6 (0.4)	-22.2 (0.4)	-2.6 (0.3)	-0.8 (0.7)	1.7 (0.8)	56	103.7	58	77	104	80	11	144	113
	B_t	18 (1)	39.1 (1.1)	45.8 (2.7)	11.8 (0.4)	-21.4 (0.2)	-24.5 (0.6)	-24.2 (0.4)	-21.2 (0.1)	-0.4 (0.8)	-0.04 (0.7)	4.5 (0.7)	17	106	13	52	167	80	11	271	157

Table 3. Results of the molecular mixing model by Nelson *et al.* 2005. The relative abundance of compound types in the occluded fractions and bulk SOM. Also, ratios of peak areas that serve as indices for soil organic matter quality.

Soil and fraction	Horizon	Relative % abundance of compound type								
		carbohydrate	nitrogenous	lignin	aliphatic material	carbonyl	char	Alkyl/O-Alkyl^	C-,H-Aryl/O-Aryl*	% Aromaticity†
Rhyolite	**A1**	8	11	8	11	7	56	0.9	3.0	10
Occluded OM	**A2**	8	7	8	17	8	51	0.8	3.0	9
	A3	10	6	5	12	7	59	1.1	3.4	6
	B_w1	17	9	10	9	7	49	2.0	3.2	13
	B_w2	21	9	14	11	6	39	2.0	3.0	20
	BC_r	22	9	17	15	8	29	1.7	2.8	25
Rhyolite	**A1**	13	11	24	17	7	28	1.0	2.1	32
Bulk SOM	**A2**	14	10	23	12	10	32	1.4	2.1	30
	A3	14	10	23	12	10	32	1.9	1.8	30
	B_w1	19	12	39	4	11	15	2.3	1.6	57
	B_w2	14	14	46	4	9	13	1.9	1.6	64
Granite	**A1**	11	6	14	33	5	30	0.6	2.6	17
Occluded OM	**A2**	9	5	7	21	6	52	0.8	3.3	8
	AC	13	5	5	19	8	50	1.0	3.3	6
Granite	**A1**	18	7	22	28	5	21	1.0	2.2	29
Bulk SOM	**A2**	18	10	26	15	5	27	1.5	2.4	36
	AC	26	10	16	20	8	20	1.5	2.0	25
Basalt	**A**	18	6	19	20	6	31	1.2	2.5	25
Occluded OM	**B_t1**	11	5	13	12	8	52	1.3	3.0	16
	B_t2	11	2	5	11	8	63	1.5	3.4	6
	B_t3	16	3	9	12	7	52	1.8	3.2	12
Basalt	**A**	25	9	26	19	4	16	1.5	2.0	40
Bulk SOM	**B_t1**	17	11	39	9	9	14	1.7	1.7	54
	B_t2	27	15	31	13	2	13	1.8	2.1	52
	B_t3	26	16	29	11	6	12	1.8	1.9	50
Dolostone	**A**	19	7	16	23	5	29	1.1	2.7	22
Occluded OM	**B_t**	17	6	16	18	5	38	1.3	2.9	21
Dolostone	**A**	25	10	18	24	5	19	1.2	2.3	27
Bulk SOM	**B_t**	21	11	20	18	8	22	1.4	2.6	30

^Decomposition is associated with an increase in alkyl C content and a drecrease in O-alkyl C content. A higher alkyl/O-alkyl ratio indicates a greater degree of decomposition (Baldock *et al.* 1997).

*The contribution of condensed aromatic structures (not lignin) to the overall content of aromatics can be demonstrated by the C-,H-aryl/O-aryl ratio.

The larger the ratio, the more charcoal is present (Dieckow et al. 2005).

†degree of aromaticity (%) was calculated as [aromatic C × 100/(alkyl C + N-alkyl/methoxyl C + O-alkyl C + aromatic C)] (Hatcher et al. 1981)

Table 4. Twenty most abundant soil organic matter pyrolysis products and their abundance in bulk soil and density/aggregate fractior
Standard errors are given in parentheses. Values are the average of 8 soil horizons (one surface and one subsurface from each site

		% Abundance			
Compound	**Class**	**Free/Light**	**Occluded**	**Mineral/Heavy**	**Bulk soil**
Methylbenzene (Toluene)	benzene	5.8 (0.7)	11.7 (1.2)	10.6 (2.9)	13.5 (2.7)
Furan-2-carbaldehyde (Furfural)	polysaccharide	9.9 (0.9)	7.4 (1.5)	4.7 (1.4)	9.5 (2.2)
Phenol	phenol	6.4 (0.8)	8.9 (0.8)	4.5 (1.2)	7.8 (1.5)
Pyridine	nitrogenous compound	1.7 (0.7)	1.6 (0.8)	11.3 (3.8)	6.6 (2.6)
Styrene (Cinnamene)	benzene	3.7 (0.7)	5.8 (0.7)	4.7 (1.2)	5.6 (0.4)
Ethanoic acid (Acetic acid)	polysaccharide	1.7 (0.5)	0 (0)	3.3 (2.5)	4.7 (2.3)
Methylpyridine (Picoline)	nitrogenous compound	1.3 (0.5)	3.0 (0.9)	11.8 (5.9)	4.1 (1.3)
Benzene	benzene	1.6 (1.1)	4.2 (1.2)	8.2 (2.9)	3.8 (0.9)
Methylphenol (Cresol)	lignin	4.1 (0.8)	4.2 (1.5)	1.9 (0.7)	3.7 (1.0)
Dimethylbenzene (Xylene)	benzene	0.4 (0.4)	1.7 (0.9)	2.7 (1.5)	3.1 (1.3)
2-Methylfuran	polysaccharide	2.2 (0.9)	2.2 (0.9)	3.5 (2.0)	3.0 (1.8)
Furan, 2,5-dimethyl-	polysaccharide	0.3 (0.3)	1.7 (1.3)	2.6 (1.3)	2.7 (1.5)
2-Furancarboxaldehyde, 5-methyl- (5-Methylfurfural)	polysaccharide	5.7 (0.5)	3.4 (1.4)	1.5 (0.8)	2.5 (0.9)
Furan	polysaccharide	1.0 (0.6)	1.4 (0.8)	2.3 (1.1)	2.3 (1.2)
1-Benzofuran (Courmarone)	polysaccharide	0.7 (0.5)	4.1 (2.1)	1.4 (0.4)	1.7 (0.4)
Phenol, 2-methoxy- (Guaiacol)	lignin	8.1 (0.9)	8.6 (1.3)	0 (0)	1.2 (0.9)
Phenol, 4-ethenyl-2-methoxy- (vinylphenol)	lignin	7.5 (1.0)	4.3 (1.2)	0 (0)	0.3 (0.3)
Alkene	lipid	3.0 (1.2)	3.0 (0.8)	0.2 (0.2)	0.2 (0.1)
Phenol, 2-methoxy-methyl- (Methylguaiacol)	lignin	3.3 (1.0)	2.6 (0.8)	0 (0)	0 (0)
Phenol, 4-Allyl-2-methoxy- (Eugenol)	lignin	1.7 (1.0)	0.8 (0.6)	0 (0)	0 (0)

Table 5. Correlations among aggregate stability model parameters and soil physiochemical characteristics.

Parameter	R^2	P value	Model
a	0.78	<0.0001	a = 40.15 + 0.53*% clay
c	0.58	0.0014	c = 77.41 - 0.94*%clay
1/b	0.74	0.0002	1/b = 127.88 - 1.75*depth
1/d	0.46	0.0099	1/d = 10666.03 - 16.82*%clay

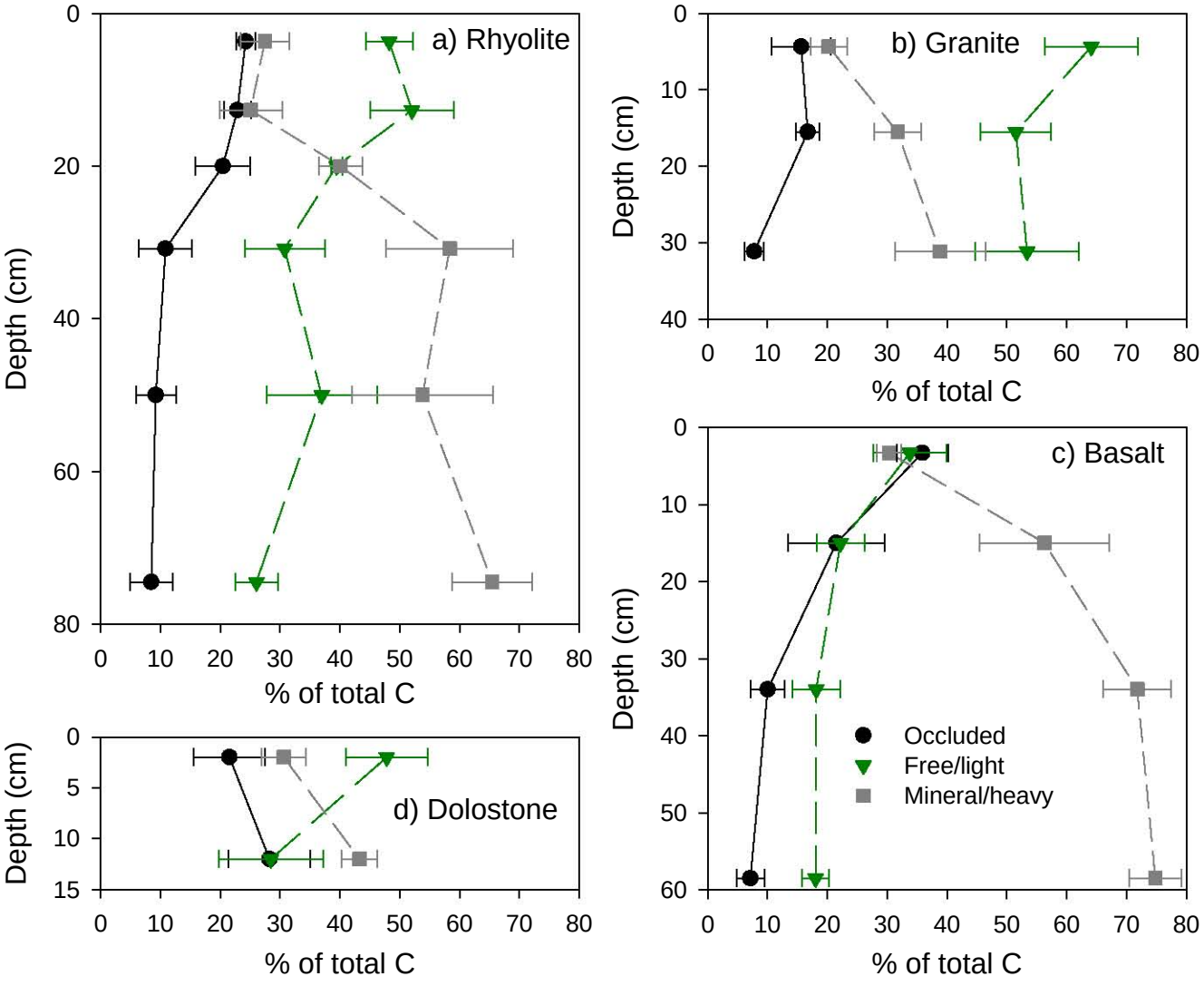
a) Rhyolite
b) Granite
c) Basalt
d) Dolostone
Depth (cm)
% of total C
Occluded
Free/light
Mineral/heavy

Figure 1.

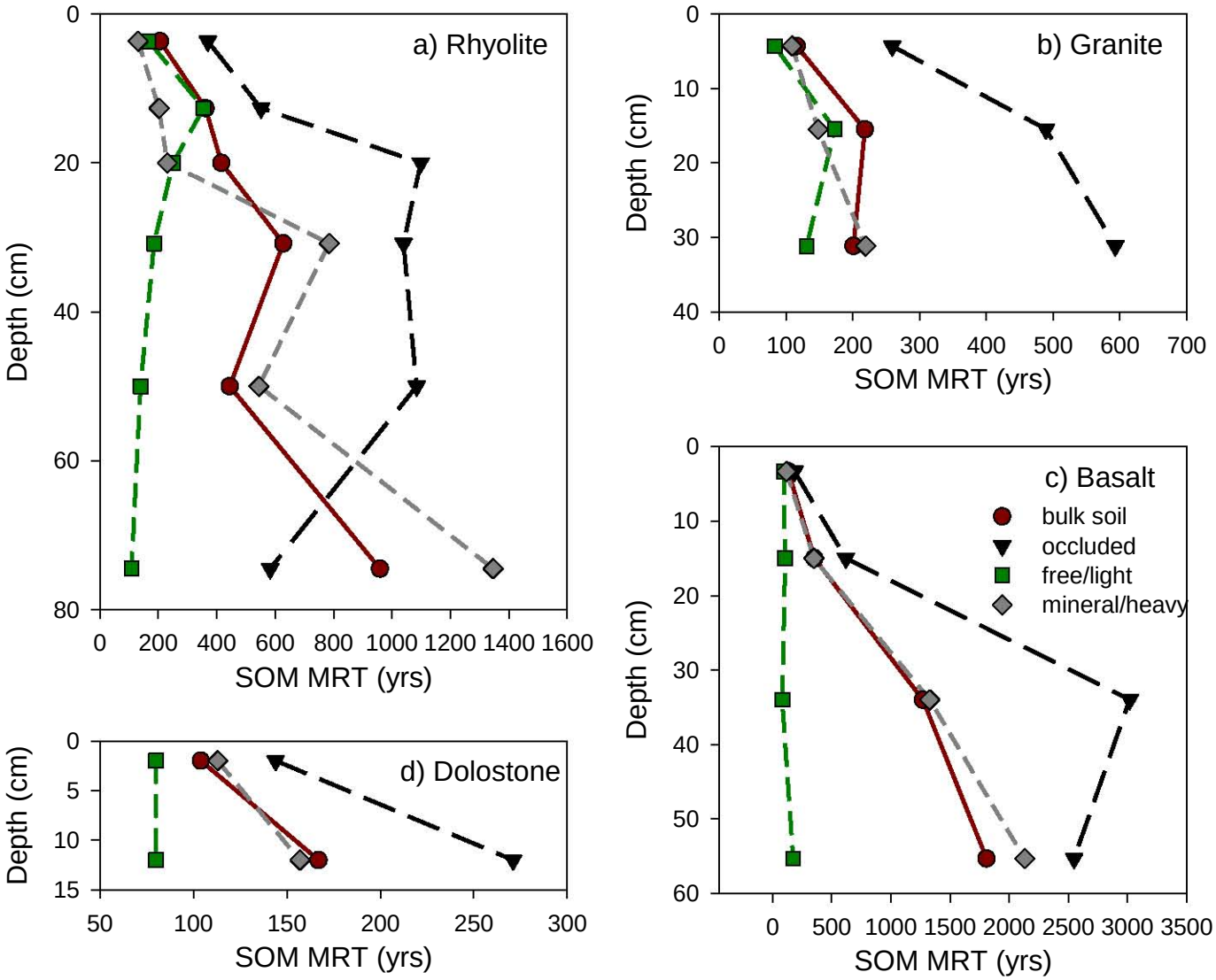
a) Rhyolite
b) Granite
c) Basalt
d) Dolostone
Depth (cm)
SOM MRT (yrs)
bulk soil
occluded
free/light
mineral/heavy

Figure 2.

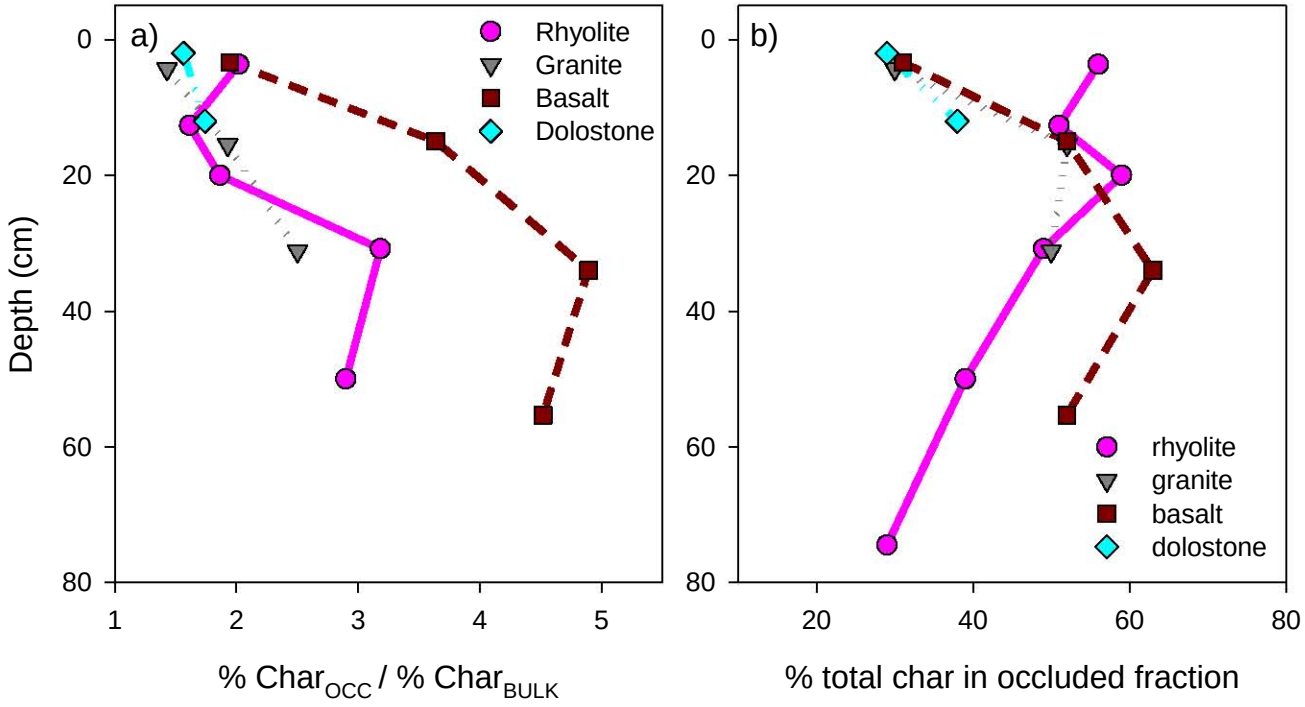
a)
Rhyolite
Granite
Basalt
Dolostone
Depth (cm)
0
20
40
60
80
1
2
3
4
5
% Char$_{OCC}$ / % Char$_{BULK}$
b)
rhyolite
granite
basalt
dolostone
20
40
60
80
% total char in occluded fraction

Figure 3.

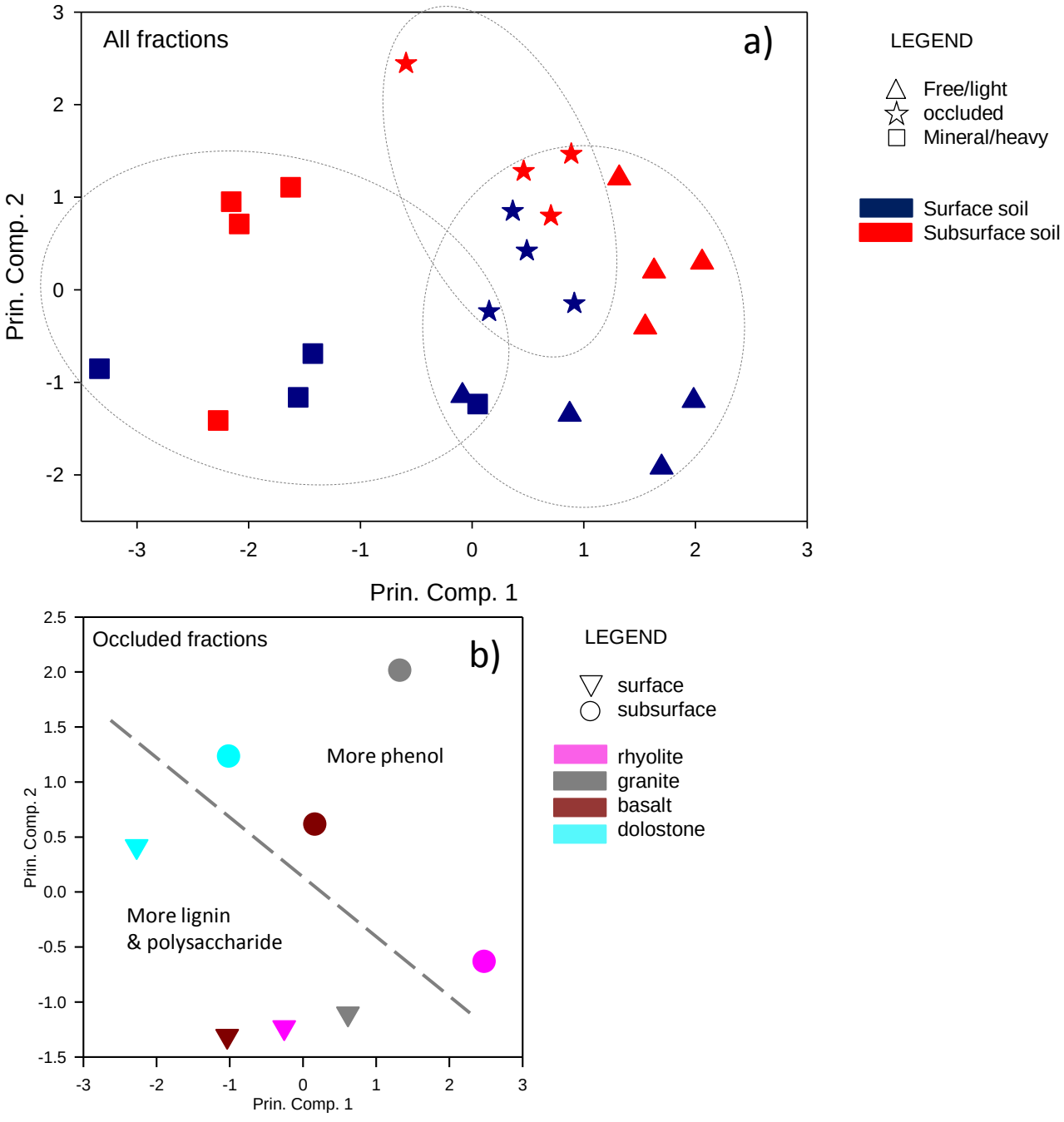
All fractions
a)
LEGEND
Free/light
occluded
Mineral/heavy
Surface soil
Subsurface soil
Prin. Comp. 2
Prin. Comp. 1
3
2
1
0
-1
-2
-3

Occluded fractions
b)
More phenol
More lignin
& polysaccharide
Prin. Comp. 2
Prin. Comp. 1
2.5
2.0
1.5
1.0
0.5
0.0
-0.5
-1.0
-1.5
-3
-2
-1
0
1
2
3

LEGEND
surface
subsurface
rhyolite
granite
basalt
dolostone

Figure 4.

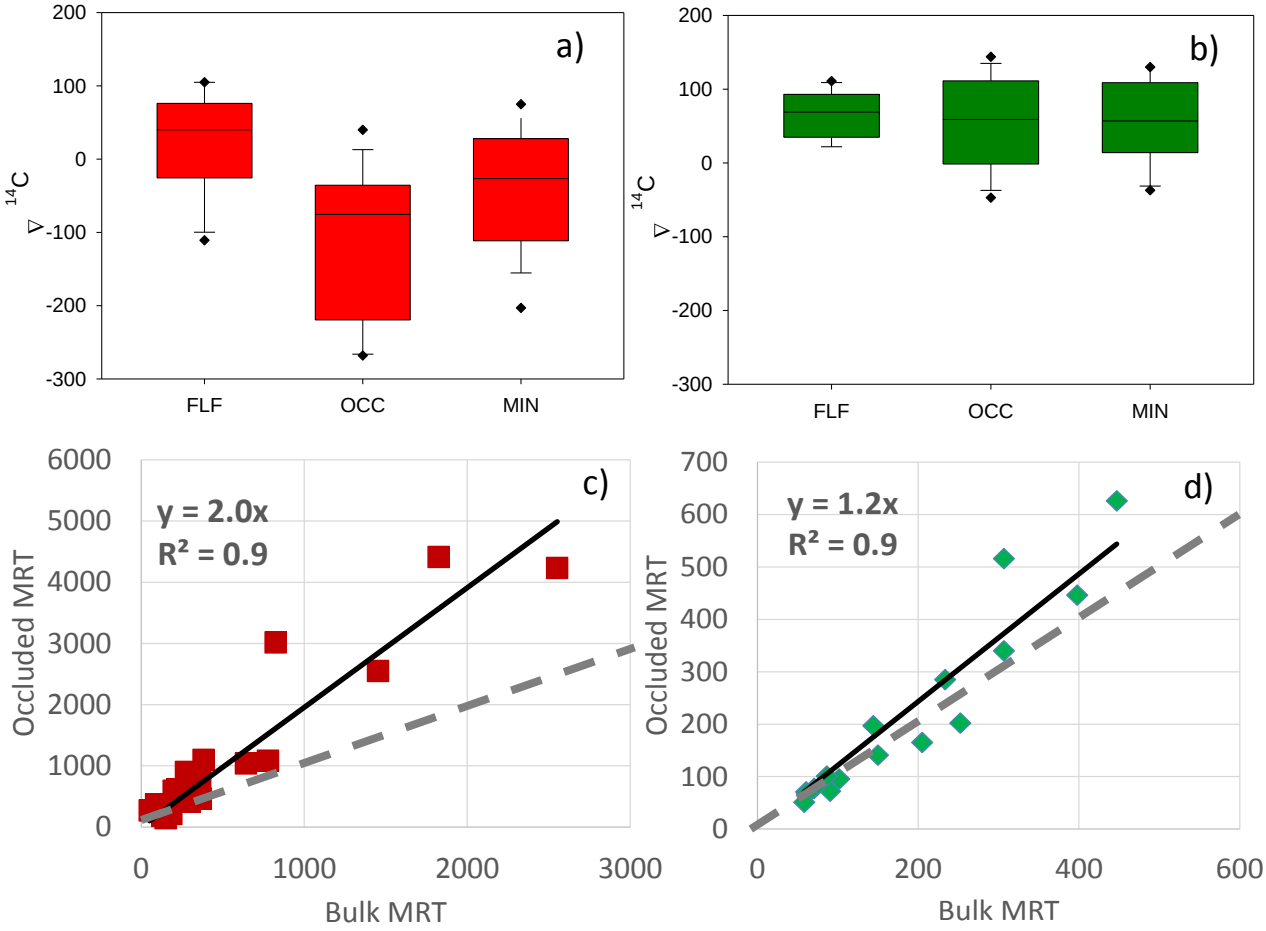
a)
b)
c)
d)
200
100
0
-100
-200
-300
Δ14C
FLF
OCC
MIN
6000
5000
4000
3000
2000
1000
0
Occluded MRT
Bulk MRT
y = 2.0x
R² = 0.9
700
600
500
400
300
200
100
y = 1.2x
R² = 0.9

Fig. 5.

Supp. Table 1. Losses of soil mass, C & N during density fractionation.

	Percent of Total Recovered (%)		
Soil	Mass	C	N
Rhyolite	102 (±1)	102 (±8)	99 (±11)
Granite	103 (±<1)	89 (±3)	84 (±10)
Basalt	101 (±1)	90 (±5)	91 (±13)
Dolostone	101 (±1)	95 (±3)	103 (±6)

Standard errors are given in parentheses.

Supp Table 2. C, N and mass of samples prior to and after HF treatment

		C/N ratio		Recovery percentage		
Parent Material	horizon	untreated	HF-treated	%C	%N	% mass
Rhyolite	A1	24.1	23.7	86	87	30.0
	A2	28.4	28.1	82	83	31.5
	A3	26.7	24.1	76	84	25.2
	B_w1	21.1	22.0	82	78	15.4
	B_w2	17.4	18.9	62	57	27.0
	BC_r	13.7	17.3	71	56	24.5
Granite	A1	32.2	39.0	78	64	48.9
	A2	32.0	27.7	72	83	45.4
	AC	26.9	25.9	72	75	31.9
Basalt	A	26.4	29.7	92	82	35.4
	B_t1	20.7	23.5	85	75	35.2
	B_t2	19.4	18.5	63	66	20.3
	B_t3	19.5	16.9	62	71	15.6
Dolostone	A	28.3	26.3	86	92	44.4
	B_t	22.7	24.3	84	79	37.7

Supp. Table 3. Radiocarbon data.

		Laboratory Sample Code*				F (Fraction modern)				^{14}C age BP			
Soil	Horizon	Bulk	Free/Light	Occluded	Mineral	Bulk	Free/Light	Occluded	Mineral	Bulk	Free/Light	Occluded	Mineral
Rhyolite	A1	AA84695	CAMS155572	CNA836	AA93067	1.1016 (0.0046)	1.0546 (0.0031)	0.9978 (0.0047)	1.0728 (0.0043)	> modern	> modern	75 ± 40	> modern
	A2	AA84696	CAMS155573	CNA837	AA93063	1.0191 (0.0042)	1.0007 (0.0030)	0.9670 (0.0032)	1.0403 (0.0042)	> modern	modern	325 ± 30	> modern
	A3	AA84697	CAMS155574	CNA838	AA93068	0.9948 (0.0042)	1.0255 (0.0032)	0.8992 (0.0035)	1.031 (0.0042)	42 ± 34	> modern	911 ± 31	> modern
	B_w1	AA84698	AA81458	CNA839	AA81460	0.9534 (0.0045)	1.0468 (0.0044)	0.9053 (0.0028)	0.9348 (0.0061)	383 ± 38	> modern	856 ± 26	542 ± 39
	B_w2	AA84699	CAMS155575	CNA840	AA93069	0.9357 (0.0042)	1.0678 (0.0031)	0.9004 (0.0029)	0.9676 (0.0065)	534 ± 35	> modern	900 ± 26	265 ± 54
	BC_r	AA84700	CAMS155576	CNA841	AA93070	0.9281 (0.0042)	1.0871 (0.0032)	0.9623 (0.0038)	0.8730 (0.0068)	599 ± 36	> modern	366 ± 32	1091 ± 62
Granite	A1	AA84701	CAMS155577	CNA842	AA93071	1.0676 (0.0044)	1.1086 (0.0033)	1.0232 (0.0032)	1.087 (0.0043)	> modern	> modern	> modern	> modern
	A2	AA84702	CAMS155578	CNA843	AA93064	1.0361 (0.0044)	1.0520 (0.0031)	0.9768 (0.0033)	1.0634 (0.0043)	> modern	> modern	246 ± 27	> modern
	AC	AA84703	AA81139	CNA844	AA81141	1.0418 (0.0043)	1.0724 (0.0045)	0.9609 (0.0047)	1.035 (0.0044)	> modern	> modern	378 ± 40	> modern
Basalt	A	AA84704	CAMS155579	CNA845	AA93072	1.0732 (0.0045)	1.0995 (0.0032)	1.0473 (0.0036)	1.0820 (0.0044)	> modern	> modern	> modern	> modern
	B_t1	AA84705	CAMS155580	CNA846	AA93066	1.0343 (0.0045)	1.0884 (0.0032)	0.9572 (0.0051)	1.0018 (0.0041)	> modern	> modern	410 ± 45	> modern
	B_t2	AA84706	AA81461	CNA847	AA81463	0.9298 (0.0063)	1.112 (0.0047)	0.7369 (0.0025)	0.8749 (0.0056)	585 ± 55	> modern	2510 ± 30	1073 ± 52
	B_t3	AA84707	CAMS155581	CNA848	AA93073	0.8624 (0.0038)	1.0515 (0.0036)	0.7703 (0.0025)	0.8025 (0.0035)	1189 ± 35	> modern	2155 ± 25	1768 ± 35
Dolostone	A	AA84693	CAMS155582	CNA849	AA93065	1.0633 (0.0073)	1.1120 (0.0048)	1.0660 (0.0032)	1.0842 (0.0043)	> modern	> modern	> modern	> modern
	B_t	AA84694	AA81455	CNA850	AA81457	1.0243 (0.0043)	1.1138 (0.0046)	1.0203 (0.0030)	1.0592 (0.0045)	> modern	> modern	> modern	> modern

* AA##### = NSF - Arizona Accelerator Mass Spectrometry Laboratory (Tucson, AZ, USA), CNA### = Centro Nacional de Aceleradores (Seville, Spain), CAMS###### = Center for Accelerator Mass Spectrometery (Livermore, CA, USA)

Supp. Table 4. Integrated areas of selected chemical shift regions, presented as % of total integrated spectral area.

Parent material/ sample type	Horizon	Chemical shift region (ppm) 245-185 carbonyl	185-160 carboxylic/amide	160-110 aryl/aromatic	110-60 O-alkyl	60-45 methoxyl-C/N-alkyl	45-0 alkyl
Rhyolite	**A1**	5.0	12.0	54.9	12.3	2.8	13.1
Occluded OM	**A2**	5.5	11.7	49.9	13.0	3.5	16.5
	A3	5.2	10.7	54.5	13.9	3.3	12.5
	B_w1	3.9	11.3	48.0	21.8	3.9	11.0
	B_w2	3.8	10.0	41.3	26.4	4.9	13.5
	BC_r	5.0	10.7	34.2	27.9	5.5	16.6
Rhyolite	**A1**	3.7	12.5	37.5	20.8	5.5	20.0
Bulk SOM	**A2**	5.5	13.8	39.7	20.7	5.2	15.2
	A3	7.7	14.5	35.2	24.3	5.5	12.9
	B_w1	5.7	14.6	33.6	28.1	6.1	12.0
	B_w2	7.9	12.7	34.3	25.5	6.4	13.2
Granite	**A1**	3.7	9.2	35.2	18.0	4.7	29.1
Occluded OM	**A2**	4.0	9.7	49.1	14.9	3.5	18.8
	AC	4.0	10.9	47.4	17.5	3.6	16.7
Granite	**A1**	3.1	9.6	30.4	24.7	6.2	25.9
Bulk SOM	**A2**	3.0	10.3	36.3	26.1	6.4	18.0
	AC	3.2	8.6	28.0	31.4	8.2	20.6
Basalt	**A**	4.3	8.8	37.6	23.4	6.3	19.6
Occluded OM	**B_t1**	5.3	10.6	51.7	16.3	3.9	12.2
	B_t2	5.3	10.0	57.0	14.8	3.1	9.8
	B_t3	4.9	9.2	50.0	20.3	4.4	11.3
Basalt	**A**	3.2	8.6	28.0	31.4	8.2	20.6
Bulk SOM	**B_t1**	6.3	12.8	31.3	26.9	7.1	15.7
	B_t2	1.8	9.2	27.4	34.4	8.2	19.1
	B_t3	4.3	10.8	25.8	32.9	8.3	18.0
Dolostone	**A**	3.4	9.2	34.4	24.3	6.6	22.1
Occluded OM	**B_t**	3.2	8.8	41.7	22.8	5.8	17.7
Dolostone	**A**	3.3	8.9	26.1	29.6	8.0	24.1
Bulk SOM	**B_t**	5.2	11.0	29.7	27.2	6.9	19.9

Supp table 5. Aggregate stability model parameters. All models were fit to three replicates per horizon.

			Model parameters: *% clay released = a(1-e^{-bx}) + c(1-e^{-dx})*					
Parent Material	horizon	Depth (cm)	a	c	b	d	1/b	1/d
			% clay released		[J (g soil)$^{-1}$]$^{-1}$		J (g soil)$^{-1}$	
Rhyolite	A1	0-5	44	66	0.007	0.001	133	778
	A2	5-14	44	68	0.010	0.001	95	845
	A3	14-24	44	93	0.014	0.001	73	1631
	B_w1	24-47	49	57	0.017	0.001	60	690
	B_w2*	47-65	53	57	0.030	0.001	35	833
Granite	A1	0-10	43	69	0.008	0.001	121	881
	A2	10-22	39	81	0.015	0.001	66	1074
Basalt	A	0-10	44	65	0.009	0.001	115	782
	B_t1	10-27	57	45	0.008	0.002	121	449
	B_t2	27-42	62	39	0.015	0.002	66	400
	B_t3	42-60	65	36	0.018	0.003	56	344
Limestone	A	0-4	42	72	0.007	0.001	153	900
	B_t	4-20	53	51	0.009	0.002	116	556

* model was fit with only 2 replicates

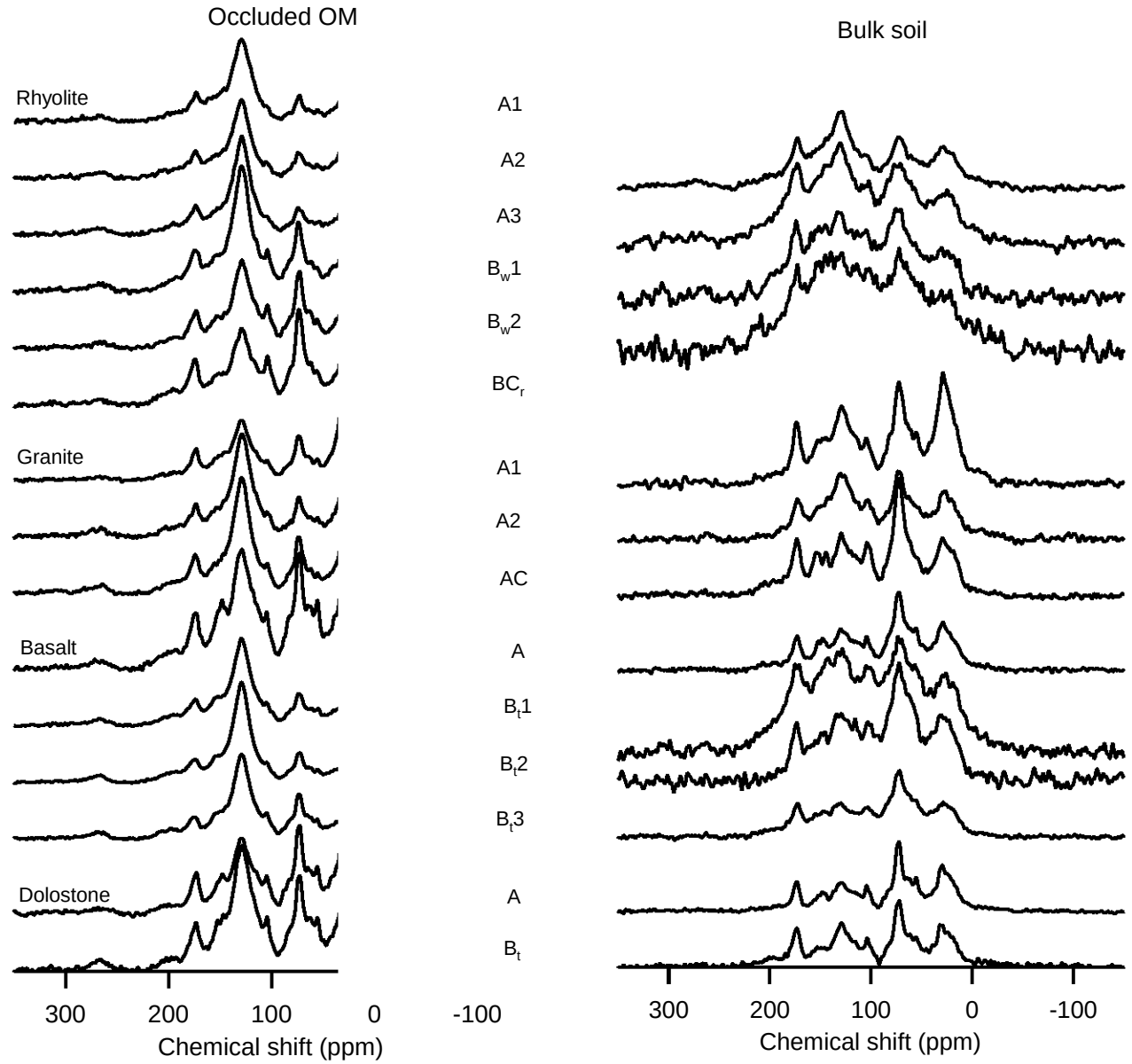

Supplementary Figure 1